ANNUAL REVIEWS

Annual Review of Physical Chemistry

Imaging Dynamic Processes in Multiple Dimensions and Length Scales

Seth L. Filbrun,[1] Fei Zhao,[1] Kuangcai Chen,[1,4] Teng-Xiang Huang,[1] Meek Yang,[3] Xiaodong Cheng,[2] Bin Dong,[3] and Ning Fang[2]

[1]Department of Chemistry, Georgia State University, Atlanta, Georgia, USA

[2]The MOE Key Laboratory of Spectrochemical Analysis and Instrumentation, State Key Laboratory of Physical Chemistry of Solid Surfaces, Innovation Laboratory for Sciences and Technologies of Energy Materials of Fujian Province (IKKEM), Xiamen Key Laboratory of Analytical Molecular Nanotechnology, College of Chemistry and Chemical Engineering, Xiamen University, Xiamen, Fujian, China; email: cxd15505@gmail.com, nfang@xmu.edu.cn

[3]Department of Chemistry and Biochemistry, University of Arkansas, Fayetteville, Arkansas, USA; email: bind@uark.edu

[4]Imaging Core Facility, Georgia State University, Atlanta, Georgia, USA

Annu. Rev. Phys. Chem. 2022. 73:377–402

First published as a Review in Advance on February 4, 2022

The *Annual Review of Physical Chemistry* is online at physchem.annualreviews.org

https://doi.org/10.1146/annurev-physchem-090519-034100

Keywords

single-particle tracking, microscopy imaging, spectroscopy, multidimensional imaging

Abstract

Optical microscopy has become an invaluable tool for investigating complex samples. Over the years, many advances to optical microscopes have been made that have allowed us to uncover new insights into the samples studied. Dynamic changes in biological and chemical systems are of utmost importance to study. To probe these samples, multidimensional approaches have been developed to acquire a fuller understanding of the system of interest. These dimensions include the spatial information, such as the three-dimensional coordinates and orientation of the optical probes, and additional chemical and physical properties through combining microscopy with various spectroscopic techniques. In this review, we survey the field of multidimensional microscopy and provide an outlook on the field and challenges that may arise.

1. INTRODUCTION

We human beings live in a multidimensional universe. Length, width, depth, and time are the four fundamental dimensions that our senses perceive macroscopically. Beyond space and time, information on matter and energy, especially the governing physical and chemical laws, forms the foundation of our understanding of the physical world. Measurement science has long been relied upon to provide all kinds of information in different length scales, from the astronomical to subatomic. At the short end of the length scales (cells, molecules, and nanomaterials), optical microscopy imaging has become an indispensable approach to understanding dynamic biological and chemical processes in complex systems. Its spatial resolution, ranging from ~200 nm governed by the diffraction limit of light to several nanometers enabled by the newly developed super-resolution imaging techniques (1–3), is sufficient to resolve many nanoscale structures and dynamics.

It is widely recognized in the imaging field that a multidimensional observation of the same sample is essential to harvest the rich properties of photons for visualizing not only the sample morphology (location, thickness, density, etc.) but also the dynamics, including motion, orientation, binding kinetics, and transient states, of target biological and chemical structures at the single-molecule level. Strictly speaking, the dimension is defined as the number of independent parameters or coordinates of an object. In the context of this discussion, a dimension can refer to different types of signals (e.g., fluorescence, scattered light, or transmitted light), color, polarization, and spatial dimensions, including translation and rotation. The term combinatorial microscopy is designated to describe this approach (4).

An active line of research in optical microscopy imaging is to integrate the state-of-the-art techniques into one system/device to provide accurate multidimensional information with high spatial and temporal resolution. This integration could be much more than a simple channel-splitting problem. Most of the advanced techniques require the nontrivial tasks involved in tuning the point-spread functions (PSFs). The PSF is the optical response of the imaging system to a point light source. Furthermore, temporal and spatial resolutions are two interconnected key parameters in optical microscopy: They share the total photons collected from the sample. In theory, researchers can sacrifice one for the other. Both are limited by the signal-to-noise (S/N) ratio. Under ideal situations, the factors governing signal and noise are determined by the nature of the samples and the detection methods; thus, they set the fundamental limits of optical microscopy.

In this review, we survey the recent efforts toward developing multidimensional imaging methodologies and systems. The following sections are organized in the sequence of an increasing number of dimensions and experimental complexity. The oldest and most practiced, multiwavelength (each color can be considered a dimension) imaging, is discussed first (Section 2.1), followed by single-particle tracking (SPT) in 3D space (Section 2.2). Then, the discussion expands to consider the dipole orientation of the imaging probes (Section 3). Finally, we survey recent efforts in combinatorial microscopy and spectroscopy techniques (Section 4). This is not a comprehensive review of all multidimensional imaging techniques but a survey of recent efforts in this emerging field.

2. CONVENTIONAL MULTIDIMENSIONAL IMAGING CONCEPTS

2.1. Multiwavelength Fluorescence Imaging

Due to good specificity and sensitivity, fluorescence microscopy is routinely used for applications in biology, chemistry, and materials science. Imaging multiple fluorophores in the same sample has become a basic requirement in many of these applications. In principle, multiwavelength imaging splits the collection pathway of the light after interacting with the sample. Dual- and quad-channel

devices are available commercially to add multiwavelength imaging capability to conventional microscopes.

Overcoming the diffraction limit with wide-field imaging techniques was a major breakthrough. Since the first demonstration of super-resolution fluorescence imaging, many labs have used this technique with multicolor systems to elucidate structures in biological and chemical systems (1, 5, 6). Shroff et al. (6) demonstrated nanometer resolution between two proteins inside fixed cells with dual-color photoactivated localization microscopy. Zhuang and coworkers (1) utilized multicolor stochastic optical reconstruction microscopy to image clathrin-coated pits and microtubules concurrently. More recently, the Zhuang lab (7, 8) developed a multicolor imaging method, namely, multiplexed error robust fluorescence in situ hybridization (MERFISH). MERFISH is a single-molecule imaging method capable of imaging thousands of RNA species in a single cell and revealing their spatial distribution. Inavalli et al. (9) developed a method that correlates stimulated emission depletion microscopy and single-molecule imaging to study the clustering of PSD95 molecules in dendritic cells. They also used this technique to study glutamate receptor mobility. Points accumulation for imaging nanoscale topography (PAINT) (10), coupled with DNA strands for labeling, that is, DNA-PAINT (11), was used to study single-molecule binding kinetics in DNA origami in real time. Frequency-multiplexed (fm)-DNA-PAINT (12) is a new method that uses a frequency modulation of the excitation lasers to excite different fluorophores, allowing for concurrent super-resolution imaging of multiple fluorophores. This frequency-modulated method works well at improving collection efficiency by removing the need for sequential excitation but requires a correction algorithm to eliminate cross talk between fluorescent probes. For additional information on multicolor single-molecule localization, readers are referred to References 3, 13, and 14.

Another broadly used multiwavelength method is Förster resonance energy transfer (FRET). Since multiwavelength single-molecule FRET was introduced (15), it has grown in usage due to its unique ability to deduce high spatial resolution in complex environments. Four-color, single-molecule FRET with total internal reflection fluorescence and confocal microscopy was demonstrated by Lee et al. (16) to reveal six interfluorophore FRET efficiencies in real time. Recently, Jeffet et al. (17) introduced a multimodal single-molecule spectromicroscopy instrument using continuously controlled spectral resolution. This instrument addition allows switching between localization, color detection, and full spectral resolution in the same channel. This is achieved by rotating two Amici prisms in the collection pathway; the angle of the prisms relative to each other changes the dispersion of light onto the camera. They demonstrated the use of this system with single-molecule FRET quantification. Single-molecule FRET was also recently demonstrated with 3D tracking (18), a technique that is discussed in the following section. For a more comprehensive review of FRET, we refer readers to References 19 and 20. Additional techniques that use multiwavelength techniques are structured illumination microscopy (21, 22) and light sheet microscopy (23, 24). This review is not exhaustive, and the reader is encouraged to read the cited excellent review articles on these techniques.

2.2. Three-Dimensional Single-Particle Tracking

SPT treats each signal as a point emission; thus, the resultant PSFs are treated similarly. Fitting the PSF to the image of a single particle/molecule has allowed nanometer-scale localization precision. By tracking single emitters' trajectories, SPT reveals rich information about specific systems in biology and materials science. There have been many good reviews giving overviews as well as providing information on the practical considerations of SPT and related data analysis (25); this section focuses on recent advances in 3D SPT (26–28).

2.2.1. Defocused imaging. One of the first methods realized for 3D particle tracking was defocused imaging (**Figure 1*a***), in which the out-of-focus ring radius is correlated to the axial position of the particle (29). This method images at a fixed focal plane and reveals the axial position of the particles relative to the imaging focal plane. Since this method was developed, there have been several other techniques developed for 3D particle tracking. Multifocal, phase mask, parallax, and astigmatism are some of the more recent methods routinely used to probe axial information in SPT imaging.

2.2.2. Confocal microscopy. In confocal microscopy, the sample is imaged using a point-scanning method. This gives a significant advantage over conventional far-field methods, as not only can the point-scanning method generate images with higher resolution, but it also produces 3D scanning capabilities. For example, Germann & Davis (30) built a four-focus excitation confocal microscope for tracking single emitters in three dimensions using a feedback mechanism and a piezo stage. They demonstrated this by tracking fluorescent nanoparticles in a glycerol solution with a 1.86-ms temporal resolution and a fluorescence photon detection efficiency of from 6% to 9%. More recently, Werner and coworkers (18) used a multicolor FRET system for 3D single-molecule tracking using a confocal microscope and a closed-loop feedback piezo stage. Welsher & Yang (31) utilized a two-photon, laser-scanning microscope with 3D target locking to visualize the cellular uptake of TAT peptide–modified nanoparticles. Furthermore, the Yang lab (32) has developed single-particle dynamic light scattering based on approximating the particles' shapes to be prolate or oblate (**Figure 1*b***). They demonstrate precision similar to transmission electron microscopy for measuring particle shape.

2.2.3. Multifocal plane microscopy. Multifocal plane far-field microscopy, which refers to imaging multiple axial planes simultaneously, is another method used to reveal 3D information. This technique splits the collected light after the objective and focuses each light path on its respective camera, each of which is conjugated to a different axial plane. Information in three dimensions is revealed by fixing the focal distance between the planes and developing a calibration curve by scanning the z axis of a fixed emitter through multiple planes. This was first demonstrated with two focal planes (**Figure 1*c***) concurrently to reveal trafficking of the Fc receptor FcRn in transfected human endothelial cells (33). More recently, a dual-objective multifocal plane microscopy system was developed for improved localization precision (34). Submillisecond temporal resolution with nanometer-level lateral and axial precision was accomplished upon tracking fluorescent beads in a glycerol solution using a bi-plane imaging system (35). Jiang et al. (36) published a dual-color bifocal imaging system by independently focusing and collimating each channel. Toprak et al. (37) demonstrated a bifocal imaging system (**Figure 1*d***) in which the image in one channel is defocused by introducing an additional focal lens for determining the axial position and the image in the second channel is kept in focus for determining the lateral position of the particle. The axial position of particles is determined by measuring the diffraction ring size.

More recently, multifocal microscopy 3D SPT has been extended to imaging up to nine focal planes concurrently. This system uses a diffractive optical element at the second pupil plane of a 4*f* system, creating nine images at different focal planes on a single camera (**Figure 1*f***) (38). Gustafsson and coworkers (39) developed an aberration-corrected multifocal system using a diffractive multifocal grating in the Fourier plane followed by a chromatic-corrected grating, and demonstrated its use by tracking single RNA polymerase II molecules inside cells with a 4-μm depth of field. Louis et al. (40) developed a multifocal plane imaging system using a proprietary prism that splits the light into eight different path lengths, thus imaging four different focal planes on each

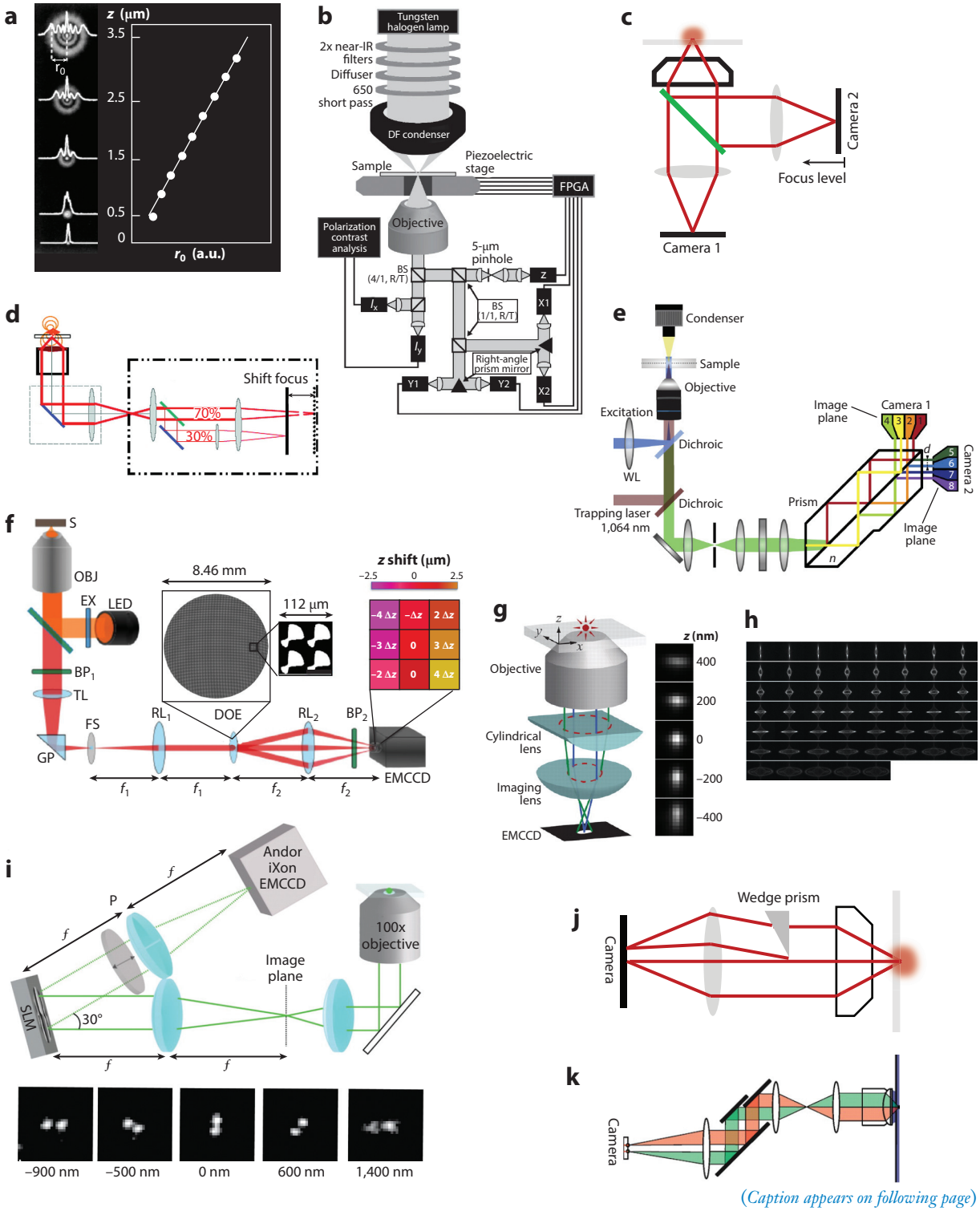

(Caption appears on following page)

Figure 1 (*Figure appears on preceding page*)

Three-dimensional single particle tracking with (*a*) diffraction ring size (r_0), (*b*) single-particle dynamic light scattering, (*c*) bi-plane imaging, (*d*) bifocal imaging, (*e*,*f*) multifocal plane imaging, (*g*,*h*) astigmatism, (*i*) double helix, and (*j*,*k*) parallax. Panel *a* adapted with permission from Reference 29; copyright 2003 Optical Society of America. Panel *b* adapted with permission from Reference 32; copyright 2019 American Chemical Society. Panel *d* adapted with permission from Reference 37; copyright 2007 American Chemical Society. Panel *e* adapted with permission from Reference 40; copyright 2020 Optical Society of America. Panel *f* adapted with permission from Reference 38; copyright 2019 American Chemical Society. Panel *g* adapted with permission from Reference 41; copyright 2008 AAAS. Panel *h* adapted with permission from Reference 44; copyright 2016 American Chemical Society. Panel *i* adapted with permission from Reference 45; copyright 2012 United States National Academy of Sciences. Panel *k* adapted with permission from Reference 49; copyright 2009 American Chemical Society. Abbreviations: BP, bandpass filter; BS, beam splitter; *d*, displacement unit; DF, dark field; DOE, diffractive optical element; EMCCD, electron multiplying charge-coupled device; EX, excitation filter; $f_{1/2}$, focal length; FPGA, field programmable gate array; FS, field stop; GP, gold prism; IR, infrared; LED, light-emitting diode; *n*, refractive index; OBJ, objective lens; RL, relay lens; SLM, spatial light modulator; TL, tube lens; WL, widefield lens.

camera for a total of eight (**Figure 1*e***). Multifocal microscopy is advantageous due to its large axial range, high imaging speed, and high accuracy, but splitting the signal into multiple channels requires major instrument customization and reduces the field of view.

2.2.4. Point-spread function engineering. Manipulating the shape of the PSF has proven to be effective at revealing axial information and tracking particles in three dimensions. For example, this can be performed by adding a cylindrical lens before the tube lens to produce astigmatism (**Figure 1*g***) (41). As the particle moves out of focus, the PSF becomes elongated faster in one lateral direction and the axial information is coded in these PSF shape changes (42). Holtzer et al. (43) demonstrated the use of astigmatism to track single quantum dots (QDs) inside cells in three dimensions with improved lateral and axial accuracy over the commonly used defocused methods. Zhao et al. (44) used a diamond-shaped astigmatism (**Figure 1*h***) for 3D tracking of fluorescent particles in cylindrical nanopores with a localization precision of 8, 12, and 15 nm in the *x*, *y*, and *z* axes, respectively, over a 5-μm imaging depth.

Another popular method of tuning the PSF is by inserting a phase mask behind the objective. The double helix PSF (**Figure 1*i***) was first established by Moerner and coworkers (45). This method transforms the original Gaussian-like PSF into a double helix shape in which the axial information is encoded in the lateral orientations of two lobes of the double helix PSF. They demonstrated the system by 3D tracking of QDs inside living cells with 10-nm localization precisions in both the lateral and axial directions (46). Recently, Shechtman et al. (47) developed a tetrapod PSF with an extended axial range of 20 μm. Phase mask methods are popular for revealing axial information and are readily available; however, they are challenging to implement in images with a high background. Furthermore, if the emitters are too dense, recovering axial information is challenging because of the overlapping of multiple engineered PSFs. Parallax imaging has also been successfully demonstrated for 3D particle tracking (48–50). This method can be achieved by inserting a wedge prism halfway into the back focal plane of the objective (**Figure 1*j***), thus slightly deviating half of the light to create two images on the same camera. The lateral image separation on the camera is related to the axial information of the sample. Yajima et al. (48) developed this method to track QDs in a motility assay, directly revealing the corkscrew rotations of a microtubule being transported on a surface functionalized with molecular motors. Chen et al. (50) has used this method to track nanorods during endocytosis—a subject that is covered in more detail in the following section. Goldman and coworkers (49) demonstrated parallax by splitting the image with a pair of almost parallel mirrors at the conjugate imaging plane to the back focal plane of the objective (**Figure 1*k***).

3. ORIENTATION ANGLES AS ADDITIONAL DIMENSIONS

In addition to wavelength and spatial coordinates, the orientation angles of anisotropic imaging probes can be considered further dimensions. The acronym SPORT, for single-particle orientation and rotational tracking, was coined to describe a toolbox for tracking the rotational dynamics of plasmonic gold nanorods (AuNRs) in live cells (51–53). The name SPORT may also refer to other SPT techniques that follow not only 3D translation but also the orientation and rotational motions of the imaging probes (53, 54). Three prominent examples of biological processes that involve rotational motion are DNA packing, self-rotation of the F_1-ATP synthase, and intracellular transport by motor proteins (55–62). Many biological molecules, especially those macromolecules that consist of multiple domains, undergo subdomain conformational changes to a specific, favorable orientation to achieve their activities (63). In SPORT experiments, there are many options for the choice of orientation probes, such as fluorescent molecules, QDs, nonfluorescent nanoparticles, Janus particles, etc. Here, we discuss different orientation probes and various optical microscopy imaging techniques used for orientation and rotational dynamics tracking studies.

3.1. Fluorescent Probes

Single-molecule, fluorescence-based techniques usually rely on either polarization modulation or PSF engineering for extracting orientation and rotational information (64–73). Here, we discuss the use of QDs as fluorescent orientation probes for rotational tracking in SPORT using single-molecule fluorescence polarization (SMFP) microscopy (64, 74–76). Readers may refer to previously published reviews for more comprehensive information (77–79).

Because of better photostability and higher quantum yield compared to those of traditional fluorescent molecules, QDs draw particular attention from researchers searching for better fluorescent orientation probes. During early studies, defocused imaging of QDs with SMFP microscopy was used along with pattern matching to simulated defocused images to determine the orientation of the probes (64, 74). A sophisticated microscopy method was also developed to simultaneously determine the movement and 3D orientation of quantum rod–tagged myosin V (76). A colocalization methodology combining interferometric scattering microscopy (iSCAT) and SMFP microscopy was reported to visualize both the position and orientation of QD-labeled Simian virus 40 (SV40) particles (75). The center of mass of each SV40 particle was imaged by iSCAT, while fluorescent QDs attached to the virus were tracked simultaneously to report the orientation in real time on artificial lipid membranes. Although the study presented an interesting methodology to investigate virus–membrane interactions, it is difficult to extend such methodology to live cell imaging, where the background inside a living cell is subject to dynamic changes.

3.2. Plasmonic Nanoparticles

Noble metal nanoparticles (also known as plasmonic nanoparticles), especially gold and silver nanoparticles, have gained exceptional attention due to their unique optical properties attributed to their localized surface plasmon resonance (LSPR) (**Figure 2*a***) (80, 81). Recent advances in optical imaging of gold nanoparticles in various applications have been reviewed elsewhere (82–86). Noble metal nanoparticles can be detected indefinitely without worrying about photobleaching or blinking. Their large optical cross section allows them to be localized with high spatial and temporal resolution (53, 81, 87). Plasmonic nanoparticles with different shapes, such as gold nanorods (AuNRs), gold nanostars, nanowires, nanocubes, nanoprisms, etc., have been explored as orientation probes (51, 88–99).

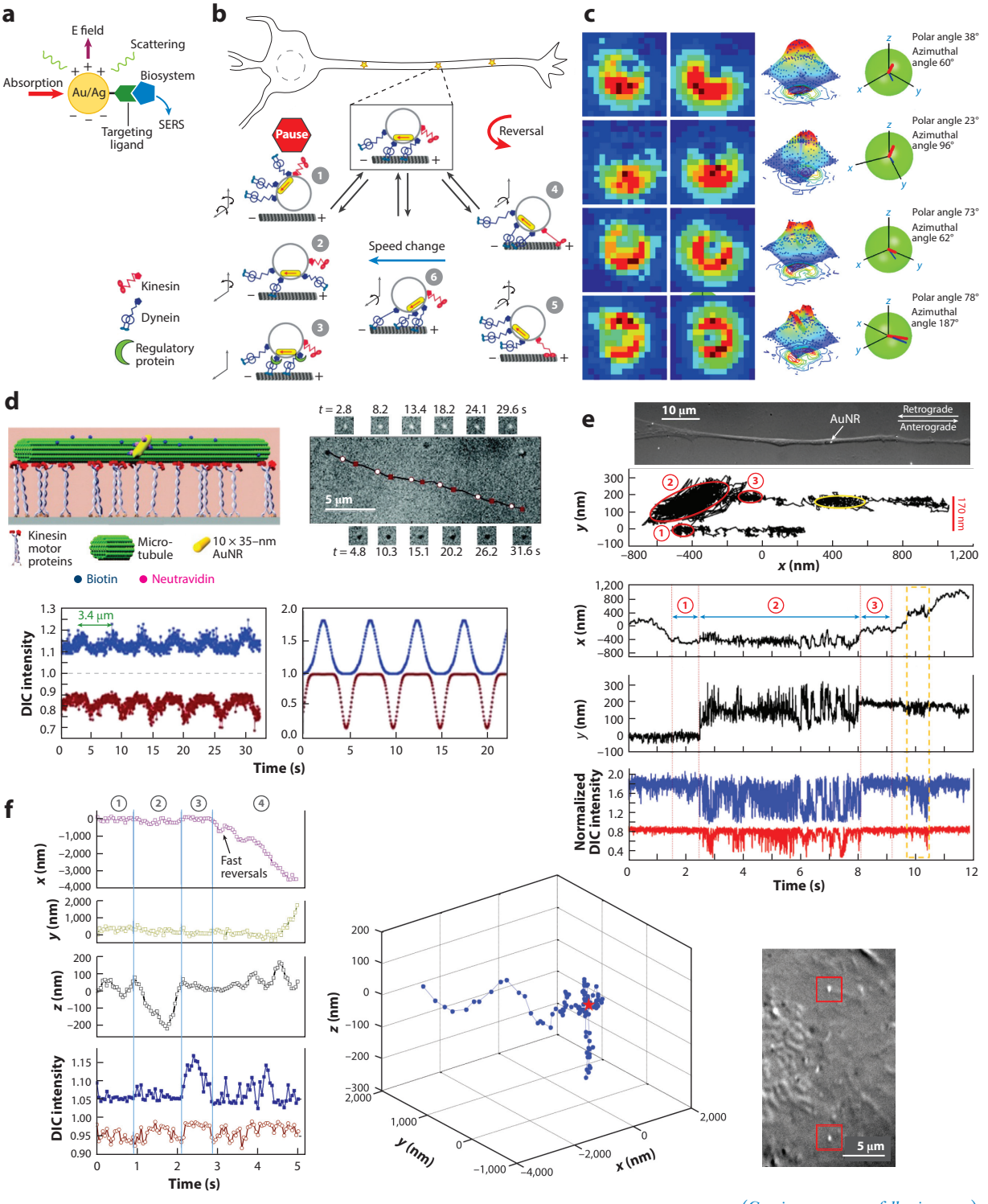

(Caption appears on following page)

Figure 2 (*Figure appears on preceding page*)

SPORT with nonfluorescent nanoparticles. (*a*) Plasmonic nanoparticles, as one unique group of nonfluorescent nanoparticles, have been explored as orientational probes with different shape variations attributed to their localized surface plasmon resonance properties. Panel *a* adapted with permission from Reference 80; copyright 2008 American Chemical Society. (*b*) Illustration of a hypothetical transporting AuNR–containing endosome with three dynein and one kinesin protein and rotational dynamics associated with the processes. Panel *b* adapted with permission from Reference 93; copyright 2018 American Association for the Advancement of Science. (*c*) Four randomly orientated AuNRs on a glass slide surface were determined by fitting recorded dark-field images (*first column*) with simulated dark-field images (*second column*). Panel *c* adapted with permission from Reference 114; copyright 2010 American Chemical Society. (*d*) Rotational motion of the microtubule was reported by (*top right*) the image pattern changes of 10 × 35–nm AuNR (*top left*) attached to its surface using DIC microscopy on engineered environments. Panel *d* adapted with permission from Reference 51; copyright 2010 American Chemical Society. (*e*, *top*) DIC image of an axon of a differentiated PC 12 cell. One of the internalized transferrin-modified AuNRs is marked by the white arrow. (*Bottom*) Trajectories and DIC intensity traces of a cargo at the track switching. Panel *e* adapted with permission from Reference 106; copyright 2012 Nature Publishing Group. (*f*) Intracellular transport of a nanorod-containing vesicle in a living A549 cell recorded by automated 5D single-particle tracking technique. Panel *f* adapted with permission from Reference 50; copyright 2017 Nature Publishing Group. Abbreviations: AuNR, gold nanorod; DIC, differential interference contrast; E field, electric field; SERS, surface-enhanced Raman spectroscopy; SPORT, single-particle orientation and rotational tracking.

3.2.1. Dark-field microscopy. AuNRs have anisotropic absorption and scattering properties accredited to the presence of both longitudinal and transverse LSPR. AuNRs show an orientation-dependent optical response when illuminated by polarized light (51, 100–102). AuNRs have proven to be one of the ideal orientation probes for studying rotational dynamics and are the most extensively used probes in SPORT experiments (51, 52, 80, 101, 103–110). AuNRs as orientation probes were first explored by Sönnichsen & Alivisatos (100) using dark-field microscopy to image AuNRs loosely attached to a surface. Dark-field microscopy was then used by many other groups (62, 93, 98, 111–115) to study the rotational dynamics of plasmonic nanoparticles. Dark-field microscopy–based SPORT techniques are not often used for live cell imaging due to high background scattering interference; however, researchers have been dedicating their efforts to finding workarounds by applying this technique to image gold nanoparticles at cell sidewalls or in axons of neurons (**Figure 2*b***) (93, 115–117). Noji and coworkers (62) developed objective-type, vertical illumination dark-field microscopy to image the rotation of single AuNRs attached to the rotary molecular motor F_1-ATPase. This study demonstrated a high-speed, angle-resolved imaging method with microsecond temporal resolution and one-degree angular precision. Defocused orientation and position imaging and multichannel polarization imaging have also been widely used in dark-field microscopy to resolve the 3D spatial position and orientation of AuNRs (**Figure 2*c***) (98, 114).

3.2.2. Total internal reflection scattering microscopy. To improve the S/N ratio and angular resolution for both azimuth and polar angles, the total internal reflection scattering (TIRS) microscopy–based focused orientation and position imaging method was developed to reveal the orientation of AuNRs on gold film in a single frame (118). This method relies on the use of linearly polarized illumination and the plasmonic coupling effect between the AuNRs and gold film to produce donut-shaped scattering patterns and determines the in-plane orientation angles in a 360° range without angular degeneracy. Dual-color TIRS microscopy was developed to illuminate the longitudinal and transverse LSPR of surface-bound AuNRs for simultaneous determination of the in-plane and out-of-plane rotational dynamics with high angular precision (119). The angular resolution of the TIRS method was further improved to subdegree uncertainty by employing a double Fresnel rhomb half-wave plate to digitally modulate the polarization of the total internal reflection (120).

3.2.3. Photothermal imaging. The Link group (101, 121) has demonstrated the use of both photothermal imaging and correlation spectroscopy to image the orientation of AuNRs. The intensity of the AuNRs was modulated by polarization using photothermal imaging (101). The orientation of the AuNRs on a glass slide surface was determined by fitting photothermal polarization traces that were confirmed by scanning electron microscopy. One-photon plasmon luminescence correlation spectroscopy was reported by the same group (121) to probe the rotational and translational dynamics of AuNRs using dual-wavelength excitation. Rotational dynamics were extracted from the polarization-dependent luminescence spectra. Zhang et al. (122) reported a similar method, called resonance light scattering correlation spectroscopy, for characterizing the rapid rotational and translational diffusion of gold nanoparticles and AuNRs in solution.

3.2.4. Differential interference contrast microscopy. Over the last decade, differential interference contrast (DIC) microscopy has been transformed from a complementary cell imaging technique into a primary research tool for visualizing the dynamics of single nanoparticles in chemical and biological applications. Wavelength-dependent DIC microscopy was explored as a multiplexing detection tool for detecting and differentiating multiple types of nanoparticles based on DIC contrast in live cells (123, 124). Wang et al. (51) laid the theoretical foundation for the use of AuNRs as orientation probes in DIC microscopy to study rotational dynamics in SPORT experiments (**Figure 2*d***). They successfully demonstrated this technique by tracking the rotational motions of AuNR cargos during transport on engineered surfaces and in live cells. The optical response of AuNRs and the influence of instrument settings on the detected DIC signal were carefully studied to investigate geometric effects (102, 125). DIC microscopy–based SPORT techniques were further applied to reveal the distinct rotational dynamics of AuNRs functionalized with different surface modifiers on live cell membranes and to visualize the rotational motion of AuNRs containing cargo at pauses (seemingly static when imaged by conventional SPT techniques) during axonal transport (**Figure 2*e***) (52, 106). These two studies shed light on the rational design of the drug delivery system and working mechanisms of motor proteins, respectively. By analogy to fluorescence polarization anisotropy, DIC polarization anisotropy was introduced as an improved approach to the direct use of bright and dark intensities for determining the orientation of the AuNRs (104, 107). This factor is computed from the orthogonally polarized dark and bright intensities in DIC traces and is believed to provide more accurate, reproducible, and reliable orientation measurements in dynamic studies. As a label-free technique, DIC does not reveal molecular information between the interaction of the AuNRs and the cellular environment. Thus, a dual-modality (DIC and fluorescence) SPORT experiment was carried out to simultaneously record the rotational motion of AuNRs and fluorescently labeled microtubules (108). DIC bright and dark intensities, as well as translational movements of the AuNRs obtained in SPORT experiments, contain rich information about the AuNRs' diffusion, rotation speed, and rotation modes, which are correlated to the transient interactions of the AuNRs and their surrounding environment (52, 109).

3.2.5. Recent advances in SPORT. New improvements to SPORT have been made through novel imaging probes (89, 126–130) and innovative instrument designs (105, 110, 131). An automated 5D SPORT system that integrates DIC and parallax microscopy has been built for continuous tracking of three spatial coordinates (x, y, z) and two orientation angles (azimuth and elevation) of the targeted AuNRs in live cellular environments (**Figure 2*f***) (50). This method was applied to reveal the characteristic rotational dynamics of transferrin-coated AuNRs from initial contact with the cell membrane, binding to membrane receptors, internalization via receptor-mediated endocytosis, and subsequent intracellular transport. To overcome the persistent challenge of

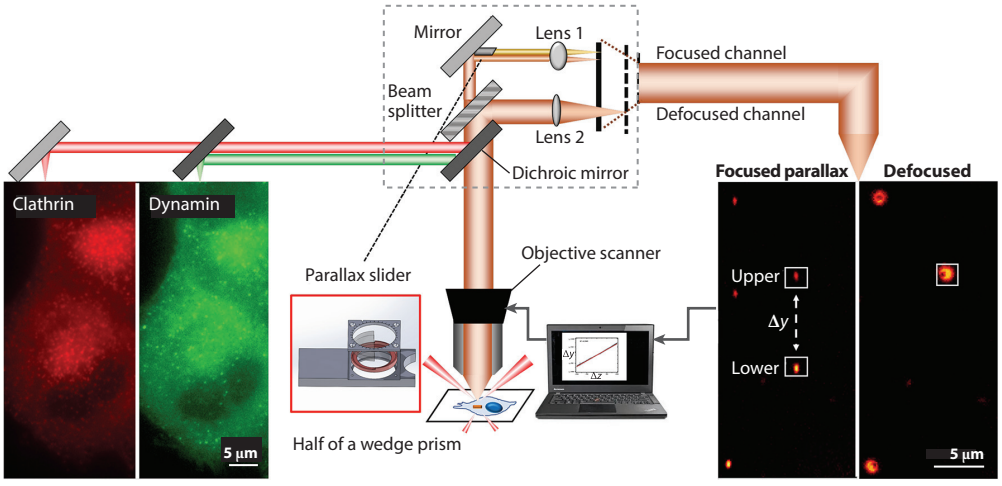

Figure 3

Multimodality automatic 5D single-particle orientation and rotational tracking (SPORT) for imaging clathrin-mediated endocytosis. Figure adapted with permission from Reference 133; copyright 2021 Nature Publishing Group.

angular degeneracy in SPORT, bifocal dark-field and parallax microscopy were integrated to expand the resolvable angle ranges: from 0 to ~360° for the azimuth angle and 0 to ~90° for the polar angle. This method was applied to study the dynamic translation and rotational motion of cargo during intracellular transport and discovered different interactions, namely, tight attachment and tethered rotation, of cargo to motor proteins and microtubule tracks (132).

Cellular processes such as clathrin-mediated endocytosis (CME) require the active participation of protein machinery. To acquire information on relevant proteins as well as the motions of nanoparticle probes, we developed a multimodality, multidimensional imaging system: two fluorescence channels for imaging clathrin and dynamin, and bifocal dark-field and parallax microscopy for automatic SPORT (**Figure 3**) (133) to study the detailed molecular mechanisms involved in CME. The synchronization of translation and the rotational motion of cargo and the assembly and disassembly of related proteins revealed how and when the cargo was cut from the membrane with rich and previously undiscovered details. Our results showed the fission of cargo is caused by the large and quick twist produced by the coordinated dynamin helix action upon GTP hydrolysis.

3.3. Janus Particles

Janus particles, named after the Roman god of gates who has two opposite faces, are a group of special particles that have two or more unique chemical and physical properties on each particle (134, 135).

3.3.1. MagMOONs. Kopelman and colleagues (136, 137) developed the Janus particles called magnetically modulated optical nanoprobes (MagMOONs) that can rotate in the magnetic field to modulate the fluorescent intensities of the optical probes. Anthony et al. (138) and Anthony & Yu (139) demonstrated the use of MagMOONs as orientation probes for tracking in four dimensions: two lateral translational motions and azimuth angle and zenith angle (also known as polar angle) (**Figure 4*a***). Nguyen & Anker (140) reported a method capable of detecting the so-called blinking, orientation-dependent fluorescence intensity changes, of MagMOONs when the particles rotate

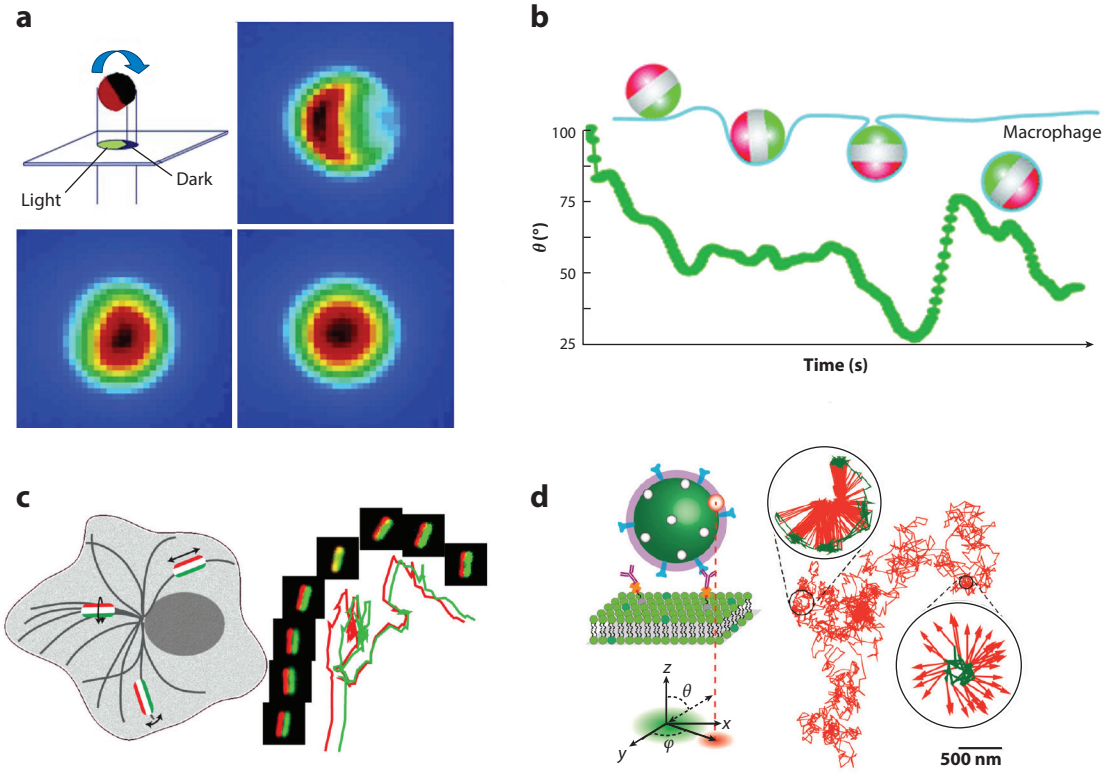

Figure 4

Single-particle orientation and rotational tracking in multiple dimensions with Janus particles. (*a*) Principle of rotational measurement using a modulated optical nanoprobe (MOON) particle with fluorescent on one side and dark on the other, and images of a 2-μm MOON particle for three orientations ranging from crescent to full moon. Panel *a* adapted with permission from Reference 138; copyright 2006 American Chemical Society. (*b*) Rotational dynamics of single triblock patchy Janus particles during phagocytosis. Panel *b* adapted with permission from Reference 142; copyright 2017 Elsevier. (*c*) Intracellular transport of rod-shaped Janus particles tightly wrapped inside endosomes. Panel *c* adapted with permission from Reference 143; copyright 2017 American Chemical Society. (*d*) Rotational and translational motions of cell membrane–coated Janus particles during ligand–receptor binding on supported lipid membranes. Panel *d* adapted with permission from Reference 146; copyright 2018 American Chemical Society.

to the external modulated magnetic field. The blinking signal changes of the MagMOONs were observed through 4-mm-thick tissue and were used to detect alginate lyase activity before and after adding alginate lyase.

3.3.2. Optically anisotropic Janus particles. In recent years, Yu and colleagues (141–147) developed several types of optically anisotropic Janus particles as orientation probes and used them for rotational tracking in different applications such as phagocytosis, intracellular transport, particle-membrane interactions, and others. In one study, microsized triblock patchy Janus particles containing two fluorescent patches on two poles were used as orientation probes to report the rotational dynamics of the single microparticles during phagocytosis (**Figure 4*b***) (142). Transient particle–cell interactions were revealed by the recorded orientation and rotation of the particles using dual fluorescence color imaging during internalization by macrophage cells. A similar method was used to fabricate rod-shaped Janus particles with two fluorescent colors on opposite sides along the long axes (**Figure 4*c***). The geometrical and optical anisotropy of these Janus

particles allow multidimensional imaging. More specifically, three rotational angles (in-plane, out-of-plane, and longitudinal) and translational motions of the endosome-wrapped single Janus particles were measured simultaneously (143).

3.3.3. Amphiphilic Janus particles. The Janus particles used in the intracellular transport studies were relatively large, which inevitably affects the rotational dynamics of cargo when used as orientation probes in live cells. Efforts have been made to fabricate Janus particles at the nanoscale with good uniformity (145–147). Amphiphilic Janus nanoparticles were constructed to study the interactions with different (charge, compositions, etc.) supported lipid bilayers (145, 147). Cell membrane–coated nanoparticles (200-nm, amine-modified green fluorescent particles conjugated to a 40-nm, carboxylate-modified red fluorescent particle on its surface) were assembled and used as orientation probes for the rotational tracking of ligand–receptor binding on supported lipid bilayers (**Figure 4*d***) (146). Distinct rotational dynamics of the nanoparticles were observed during receptor binding, which was hidden in translational confined interactions. With the advances in anisotropic Janus particle fabrication, new types of Janus particles will no doubt emerge for rotational studies in different fields.

4. INTEGRATION OF SPECTROSCOPIC AND MICROSCOPIC MEASUREMENTS

Beyond the dimensions of color, position, and orientation, it is critical to reveal the evolution of physicochemical properties of the sample and to identify chemical species that are consumed and/or produced during dynamic processes. Spectroscopic measurements, such as Raman, infrared (IR), absorption, and fluorescence, provide chemical information. The combination of spectroscopic and microscopic measurements reveals a more thorough picture of the system. Microscopic and spectroscopic measurements of the same sample are typically done with separate instruments (148, 149). This severely limits the correlation of microscopic and spectroscopic information for dynamic processes. Different aspects (dimensions) of the sample undergo change during a dynamic process on different time and length scales; for example, in a catalytic reaction, fast changes occur in the reaction kinetics and long-term changes occur in the catalyst stability and degradation. This corresponds to nanoscale changes of the catalyst structure and meso- or microscale changes to the catalyst dispersion or support (150). Thus, the integration of the spectroscopic and microscopic techniques is vital to obtaining correlated information for a more comprehensive understanding on the sample of interest. Here, we provide a brief review of the recent examples of integrated spectromicroscopy techniques.

Raman spectroscopy is a vibrational spectroscopic technique capable of providing molecular fingerprint information for chemical identification and revealing the structural and electronic properties of materials. Raman spectroscopy has been successfully integrated with different optical microscopies (151–154). Single-particle Raman spectroscopy has been integrated with scattering imaging and an optical trapping system (**Figure 5*a***) to realize concurrent characterization of the physical and chemical properties of single particles (151). The orchestrated combination of Raman spectroscopy measurements and fluorescence imaging has been applied to the investigation of biological systems such as the therapeutic effects of drugs in vivo and the diagnosis of tumors (152, 153). The integration of Raman spectroscopy with a multiphoton imaging system (**Figure 5*b***) helps to characterize the molecular origin of detected multiphoton-induced signals and to correlate the image contrast with specific tissue constituents (154).

IR spectroscopy is another nondestructive spectroscopic technique providing rich chemical and structural information. It has also been used with Raman spectroscopy to provide

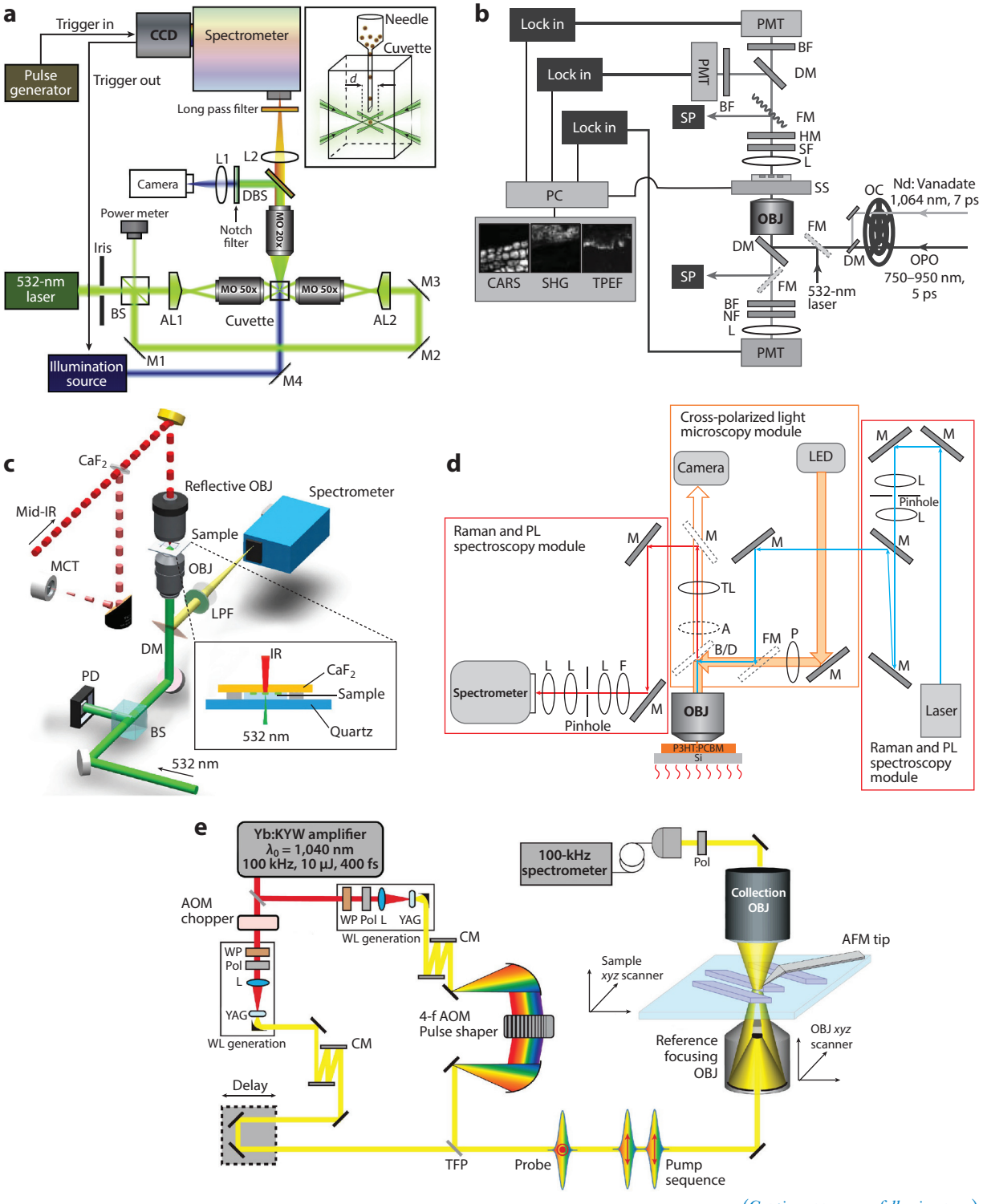

(Caption appears on following page)

Figure 5 (*Figure appears on preceding page*)

Examples of integrated spectroscopy and microscopy measurements. (*a*) Experimental setup of the optical trapping–Raman spectroscopy system. Panel *a* adapted with permission from Reference 151; copyright 2018 Elsevier. (*b*) Schematic diagram of the multimodal spectromicroscopy system. Panel *b* adapted with permission from Reference 154; copyright 2008 The Optical Society. (*c*) Schematic of the IR Raman microscope. Panel *c* adapted with permission from Reference 164; copyright 2019 American Chemical Society. (*d*) Schematic diagram of the spectromicroscopy system for studying the dynamic processes in thin film during thermal annealing. Panel *d* adapted with permission from Reference 175; copyright 2020 American Chemical Society. (*e*) Experimental schematic of the two-dimensional WL microscopy system. Panel *e* adapted with permission from Reference 178; copyright 2019 American Chemical Society. Abbreviations: AFM, atomic force microscope; AL, Axicon lens; AOM, acousto-optic modulator; B/D, beam splitter/dichroic mirror; BF, bandpass filter; BS, beam splitter; CARS, coherent anti-stokes Raman spectroscopy; CCD, charge-coupled device; CM, chirped mirror; DBS, dichroic beam splitter; DM, dichroic mirror; FM, flip mirror; HM, hot mirror; IR, infrared; L, lens; LED, light-emitting diode; LPF, long pass filter; M, mirror; MCT, mercury cadmium telluride detector; MO, micro-objective; NF, notch filter; OBJ, objective lens; OC, optical chopper; OPO, optical parametric oscillator; P, prism; PC, personal computer; PD, photo diode; PL, photoluminescence; PMT, photomultiplier tube; Pol, polarizer; SF, short pass filter; SHG, second harmonic generation; SP, spectrograph; SS, scanning stage; TFP, thin film polarizer; TL, tube lens; TPEF, two-photon excited fluorescence; WL, white light; WP, waveplate; YAG, yttrium aluminum garnet; Yb:KYW, Yb-doped potassium yttrium tungstate.

complementary information for the same sample on different instruments (155–158). However, poor spatial resolution of IR spectroscopy, in the range of from 3 to 30 μm (159), limits its application in imaging. In IR photothermal imaging, which was developed to overcome this poor spatial resolution (160–163), the resolution is determined by the diffraction limit of the visible probe wavelength. The further integration of mid-IR photothermal microscopy with confocal Raman spectroscopy (**Figure 5*c***) (164) has realized fast-IR photothermal imaging of living cells with submicrometer resolution, accompanied with full-spectrum Raman and photothermal spectra.

Fluorescence super-resolution microscopy has been widely integrated with fluorescence emission spectroscopy to realize multicolor or true color imaging. In early studies, fluorescence spectroscopic information was revealed using the photon count ratio detected by two collection channels covering different wavelength regions and was used to separate signals from different markers (165–167). Excitation and activation lasers are reflected by a dichroic mirror and are focused onto the back focal plane of the objective, providing wide-field illumination. The fluorescence signal from switch-on molecules is split into two light paths according to wavelength and is detected by the different areas on an electron multiplying charge-coupled device (EMCCD) detector. In recent studies, the fluorescence spectroscopic information is obtained by dispersing the fluorescence signal through a prism before detection by one of the collection channels (168–171). With these advances, high-throughput, single-molecule spectroscopy combined with super-resolution microscopy that uses a prism in one of the detection channels achieves the recording of the spectra of $\sim 10^2$ molecules per few-millisecond time period, and every molecule can be characterized both spatially and spectrally in 3D (168). There are also studies replacing the prism with a grating and realizing simultaneous spatial and spectral characterization (172, 173). The new dimension of fluorescence spectral information is used to investigate physicochemical changes of local environments (171, 173) and reaction pathways of single molecules (174).

Photoluminescence (PL) is light emission from matter after absorption of photons. PL spectroscopy is a noncontact, nondestructive method that can investigate the optical and electronic band properties of matter. Recently, Fang and colleagues (175) developed a multimodality spectromicroscopy imaging system combining far-field, cross-polarized light microscopy with confocal Raman and photoluminescence spectroscopy (**Figure 5*d***). They used this to study the annealing process of bulk heterojunction polymers prepared on reflective surfaces in situ. The uniqueness of this imaging system is its ability to add home-built sample stages, such as the thermal annealing stage used in this study. The addition of sample stages, tuning the dynamics of the system, gives further dimensionality to the system, providing rich information about the sample of interest.

Transient absorption (TA) spectroscopy is a widely applied spectroscopy method that provides valuable insights into the dynamics of excited-state molecules (176). Zanni and colleagues (177, 178) developed a multimodal 2D white-light microscopy system that combines atomic force microscopy (AFM) and 2D electronic spectroscopy using a broadband, white-light, supercontinuum laser, for both pump-probe and broadband transient absorption imaging, realizing multidimensional spectroscopic measurements with high temporal and spectral resolution and spatial dimensions along with hyperspectral transient absorption images (**Figure 5*e***). This characterization technique first identifies and topographically characterizes individual nanostructures using AFM, then spatially and spectrally maps the nanostructure's intrinsic ultrafast response using TA imaging and high-resolution 2D electronic spectroscopy.

5. SUMMARY AND OUTLOOK

This review discusses the recent advances in optical microscopy and spectroscopy to extract multidimensional information from the sample, including morphological features, chemical structure and dynamics, and physical motions (**Figure 6**). Further improvement of multidimensional imaging in a variety of applications is still needed.

Acquiring multidimensional data simultaneously for dynamic processes remains challenging. In situ imaging under realistic conditions may suffer from insufficient spatial and temporal resolution to distinguish individual molecules involved in a reaction or to follow chemical bond formation. Therefore, it is very important to increase the spatial resolution and sensitivity of the imaging method. Fluorescence super-resolution microscopy is the typical optical microscopy that can overcome the diffraction limit of light and provides a spatial resolution of ~10 nm. IR photothermal imaging was developed to overcome the poor spatial resolution of conventional IR microscopy (160, 163). Further efforts should be devoted to developing the new imaging

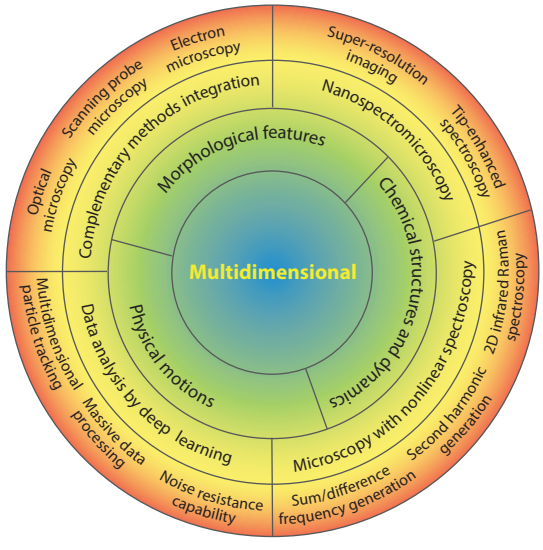

Figure 6

Multidimensional optical microscopy and spectroscopy analysis.

principles. Furthermore, spectroscopies with high spatial resolution would be better to integrate with microscopy. Tip-enhanced spectroscopies, such as tip-enhanced Raman spectroscopy (179–181), tip-enhanced photoluminescence spectroscopy (182, 183), and nanoscale IR spectroscopy (184, 185), have high spatial resolution down to 10 nm (186) in air and subnanometer (187) under ultrahigh vacuum. These spectroscopies can provide chemical information from small nanostructures, such as defects. However, it is still greatly challenging to combine tip-enhanced spectroscopies with microscopy.

Continuous efforts are needed to gain new dimensions through the integration of complementary imaging techniques. As an example, the combination of multidimensional optical imaging with electron microscopy is a powerful approach for extracting dynamic and localization information from optical microscopy with detailed 3D structural information from electron microscopy, i.e., 4D cryo-electron microscopy, with time being the fourth dimension (188). Furthermore, scanning probe microscopy (SPM), such as atomic force microscopy (AFM) and scanning tunneling microscopy, can study morphology, phase transformation, and electronic properties of surfaces with down to atomic resolution. High-speed SPM has made it possible to directly visualize dynamic processes. For example, high-speed AFM has been used to reveal subsecond dynamics of cardiac thin filaments upon Ca^{2+} activation and heavy meromyosin binding (189). The integration of SPM can lead to new dimensions of multidimensional optical imaging.

Until now, most of the spectroscopy integrated into microscopy is linear spectroscopy. Spectroscopy in 2D, which measures the nonlinear third-order response function, has high structural sensitivity and intrinsic time resolution to characterize the structural and dynamic information of samples (190). This achieves improved resolution of neighboring peaks compared to conventional linear spectroscopies, resulting from the nonlinear scaling of the intensity with transition dipole strength (191, 192). Techniques such as 2D IR spectroscopy, 2D electronic spectroscopy (193), and 2D Raman-THz (194, 195) and 2D IR-Raman spectroscopies (196) have been developed. Besides 2D spectroscopy, the other nonlinear spectroscopies, such as second harmonic generation, sum frequency generation, and difference frequency generation, are also important for the wider application of multidimensional optical imaging.

Data analysis in multidimensional imaging is another area that requires immediate attention. Increasing the number of dimensions dramatically increases the amount and complexity of data produced and archived. The information buried in the interrelationships among the dimensions scales up exponentially as the number of dimensions increases. Furthermore, multiple dimensions commonly share the same pool of photons, so splitting them into collection channels may decrease the image quality significantly; therefore, robust data analysis algorithms will be greatly needed. In this regard, fast-developing, deep-learning algorithms may be key to extending our capabilities in interpreting the data. The main concept of deep learning is to extract high-level, complex abstractions as data representations through a hierarchical learning process. Compared to conventional shallow learning, deep learning generalizes in both nonlocal and global methods, generating learning patterns and relationships beyond immediate neighbors in the data. Because of this, it can be used to extract complex patterns from massive amounts of interconnected data. Deep-learning algorithms can potentially be a valuable tool in multidimensional data analysis. In fact, we have started to see achievements in some areas. These include the algorithms that connect dots between frames in the presence of many particles for particle tracking (197). In 3D imaging, deep neural networks have demonstrated their noise-resistance capability for pattern recognition–based z-position recovery (198). This makes them effective at minimizing the impact of high background noise. They have also been used for augmented microscopy, which extracts latent information from obscure bright-field images with the help of the parallel fluorescence images (199). Deep learning is expected to play a more important role in the future.

DISCLOSURE STATEMENT

The authors are not aware of any affiliations, memberships, funding, or financial holdings that might be perceived as affecting the objectivity of this review.

ACKNOWLEDGMENTS

N.F. and X.C. acknowledge support from Science and Technology Projects of Innovation Laboratory for Sciences and Technologies of Energy Materials of Fujian Province (IKKEM) (RD2020050501). M.Y. and B.D. acknowledge funding support from the University of Arkansas. S.L.F., F.Z., K.C., and T.-X.H. acknowledge support from Georgia State University. X.C. acknowledges support from the China Postdoctoral Science Foundation (2021M700114).

LITERATURE CITED

1. Bates M, Huang B, Dempsey GT, Zhuang X. 2007. Multicolor super-resolution imaging with photo-switchable fluorescent probes. *Science* 317:1749–53
2. Manley S, Gillette JM, Patterson GH, Shroff H, Hess HF, et al. 2008. High-density mapping of single-molecule trajectories with photoactivated localization microscopy. *Nat. Methods* 5:155
3. Huang B, Bates M, Zhuang X. 2009. Super-resolution fluorescence microscopy. *Annu. Rev. Biochem.* 78:993–1016
4. Axelrod D, Omann GM. 2006. Combinatorial microscopy. *Nat. Rev. Mol. Cell Biol.* 7:944–52
5. Donnert G, Keller J, Wurm CA, Rizzoli SO, Westphal V, et al. 2007. Two-color far-field fluorescence nanoscopy. *Biophys. J.* 92:L67–69
6. Shroff H, Galbraith CG, Galbraith JA, White H, Gillette J, et al. 2007. Dual-color superresolution imaging of genetically expressed probes within individual adhesion complexes. *PNAS* 104:20308–13
7. Chen KH, Boettiger AN, Moffitt JR, Wang S, Zhuang X. 2015. Spatially resolved, highly multiplexed RNA profiling in single cells. *Science* 348:aaa6090
8. Moffitt JR, Hao J, Wang G, Chen KH, Babcock HP, Zhuang X. 2016. High-throughput single-cell gene-expression profiling with multiplexed error-robust fluorescence in situ hybridization. *PNAS* 113:11046–51
9. Inavalli VVGK, Lenz MO, Butler C, Angibaud J, Compans B, et al. 2019. A super-resolution platform for correlative live single-molecule imaging and STED microscopy. *Nat. Methods* 16:1263–68
10. Sharonov A, Hochstrasser RM. 2006. Wide-field subdiffraction imaging by accumulated binding of diffusing probes. *PNAS* 103:18911–16
11. Jungmann R, Steinhauer C, Scheible M, Kuzyk A, Tinnefeld P, Simmel FC. 2010. Single-molecule kinetics and super-resolution microscopy by fluorescence imaging of transient binding on DNA origami. *Nano Lett.* 10:4756–61
12. Gómez-García PA, Garbacik ET, Otterstrom JJ, Garcia-Parajo MF, Lakadamyali M. 2018. Excitation-multiplexed multicolor superresolution imaging with fm-STORM and fm-DNA-PAINT. *PNAS* 115:12991–96
13. van Wee R, Filius M, Joo C. 2021. Completing the canvas: advances and challenges for DNA-PAINT super-resolution imaging. *Trends Biochem. Sci.* 46:918–30
14. Lelek M, Gyparaki MT, Beliu G, Schueder F, Griffié J, et al. 2021. Single-molecule localization microscopy. *Nat. Rev. Methods Primers* 1:39
15. Hohng S, Joo C, Ha T. 2004. Single-molecule three-color FRET. *Biophys. J.* 87:1328–37
16. Lee J, Lee S, Ragunathan K, Joo C, Ha T, Hohng S. 2010. Single-molecule four-color FRET. *Angew. Chem. Int. Ed.* 49:9922–25
17. Jeffet J, Ionescu A, Michaeli Y, Torchinsky D, Perlson E, et al. 2021. Multimodal single-molecule microscopy with continuously controlled spectral resolution. *Biophys. Rep.* 1:100013
18. Keller AM, DeVore MS, Stich DG, Vu DM, Causgrove T, Werner JH. 2018. Multicolor three-dimensional tracking for single-molecule fluorescence resonance energy transfer measurements. *Anal. Chem.* 90:6109–15

19. Hohng S, Lee S, Lee J, Jo MH. 2014. Maximizing information content of single-molecule FRET experiments: multi-color FRET and FRET combined with force or torque. *Chem. Soc. Rev.* 43:1007–13
20. Bartels K, Lasitza-Male T, Hofmann H, Löw C. 2021. Single-molecule FRET of membrane transport proteins. *ChemBioChem* 22:2657–71
21. Heintzmann R, Huser T. 2017. Super-resolution structured illumination microscopy. *Chem. Rev.* 117:13890–908
22. Wu Y, Shroff H. 2018. Faster, sharper, and deeper: structured illumination microscopy for biological imaging. *Nat. Methods* 15:1011–19
23. Wan Y, McDole K, Keller PJ. 2019. Light-sheet microscopy and its potential for understanding developmental processes. *Annu. Rev. Cell Dev. Biol.* 35:655–81
24. Girkin JM, Carvalho MT. 2018. The light-sheet microscopy revolution. *J. Opt.* 20:053002
25. Aaron J, Wait E, DeSantis M, Chew T-L. 2019. Practical considerations in particle and object tracking and analysis. *Curr. Protoc. Cell Biol.* 83:e88
26. von Diezmann A, Shechtman Y, Moerner WE. 2017. Three-dimensional localization of single molecules for super-resolution imaging and single-particle tracking. *Chem. Rev.* 117:7244–75
27. Shen H, Tauzin LJ, Baiyasi R, Wang W, Moringo N, et al. 2017. Single particle tracking: from theory to biophysical applications. *Chem. Rev.* 117:7331–76
28. Zhong Y, Wang G. 2020. Three-dimensional single particle tracking and its applications in confined environments. *Annu. Rev. Anal. Chem.* 13:381–403
29. Speidel M, Jonáš A, Florin E-L. 2003. Three-dimensional tracking of fluorescent nanoparticles with subnanometer precision by use of off-focus imaging. *Opt. Lett.* 28:69–71
30. Germann JA, Davis LM. 2014. Three-dimensional tracking of a single fluorescent nanoparticle using four-focus excitation in a confocal microscope. *Opt. Express* 22:5641–50
31. Welsher K, Yang H. 2014. Multi-resolution 3D visualization of the early stages of cellular uptake of peptide-coated nanoparticles. *Nat. Nanotechnol.* 9:198–203
32. Guerra LF, Muir TW, Yang H. 2019. Single-particle dynamic light scattering: shapes of individual nanoparticles. *Nano Lett.* 19:5530–36
33. Prabhat P, Ram S, Ward ES, Ober RJ. 2004. Simultaneous imaging of different focal planes in fluorescence microscopy for the study of cellular dynamics in three dimensions. *IEEE Trans. NanoBiosci.* 3:237–42
34. Ram S, Prabhat P, Ward ES, Ober RJ. 2009. Improved single particle localization accuracy with dual objective multifocal plane microscopy. *Opt. Express* 17:6881–98
35. Juette MF, Bewersdorf J. 2010. Three-dimensional tracking of single fluorescent particles with submillisecond temporal resolution. *Nano Lett.* 10:4657–63
36. Jiang C, Kaul N, Campbell J, Meyhofer E. 2017. A novel dual-color bifocal imaging system for single-molecule studies. *Rev. Sci. Instrum.* 88:053705
37. Toprak E, Balci H, Blehm BH, Selvin PR. 2007. Three-dimensional particle tracking via bifocal imaging. *Nano Lett.* 7:2043–45
38. Wang X, Yi H, Gdor I, Hereld M, Scherer NF. 2019. Nanoscale resolution 3D snapshot particle tracking by multifocal microscopy. *Nano Lett.* 19:6781–87
39. Abrahamsson S, Chen J, Hajj B, Stallinga S, Katsov AY, et al. 2013. Fast multicolor 3D imaging using aberration-corrected multifocus microscopy. *Nat. Methods* 10:60–63
40. Louis B, Camacho R, Bresolí-Obach R, Abakumov S, Vandaele J, et al. 2020. Fast-tracking of single emitters in large volumes with nanometer precision. *Opt. Express* 28:28656–71
41. Huang B, Wang W, Bates M, Zhuang X. 2008. Three-dimensional super-resolution imaging by stochastic optical reconstruction microscopy. *Science* 319:810–13
42. Kao HP, Verkman A. 1994. Tracking of single fluorescent particles in three dimensions: use of cylindrical optics to encode particle position. *Biophys. J.* 67:1291–300
43. Holtzer L, Meckel T, Schmidt T. 2007. Nanometric three-dimensional tracking of individual quantum dots in cells. *Appl. Phys. Lett.* 90:053902
44. Zhao L, Zhong Y, Wei Y, Ortiz N, Chen F, Wang G. 2016. Microscopic movement of slow-diffusing nanoparticles in cylindrical nanopores studied with three-dimensional tracking. *Anal. Chem.* 88:5122–30

45. Backlund MP, Lew MD, Backer AS, Sahl SJ, Grover G, et al. 2012. Simultaneous, accurate measurement of the 3D position and orientation of single molecules. *PNAS* 109:19087–92
46. Thompson MA, Lew MD, Badieirostami M, Moerner WE. 2010. Localizing and tracking single nanoscale emitters in three dimensions with high spatiotemporal resolution using a double-helix point spread function. *Nano Lett*. 10:211–18
47. Shechtman Y, Weiss LE, Backer AS, Sahl SJ, Moerner WE. 2015. Precise three-dimensional scan-free multiple-particle tracking over large axial ranges with tetrapod point spread functions. *Nano Lett*. 15:4194–99
48. Yajima J, Mizutani K, Nishizaka T. 2008. A torque component present in mitotic kinesin Eg5 revealed by three-dimensional tracking. *Nat. Struct. Mol. Biol.* 15:1119–21
49. Sun Y, McKenna JD, Murray JM, Ostap EM, Goldman YE. 2009. Parallax: high accuracy three-dimensional single molecule tracking using split images. *Nano Lett*. 9:2676–82
50. Chen K, Gu Y, Sun W, Bin D, Wang G, et al. 2017. Characteristic rotational behaviors of rod-shaped cargo revealed by automated five-dimensional single particle tracking. *Nat. Commun.* 8:887
51. Wang G, Sun W, Luo Y, Fang N. 2010. Resolving rotational motions of nano-objects in engineered environments and live cells with gold nanorods and differential interference contrast microscopy. *J. Am. Chem. Soc.* 132:16417–22
52. Gu Y, Sun W, Wang G, Fang N. 2011. Single particle orientation and rotation tracking discloses distinctive rotational dynamics of drug delivery vectors on live cell membranes. *J. Am. Chem. Soc.* 133:5720–23
53. Stender AS, Marchuk K, Liu C, Sander S, Meyer MW, et al. 2013. Single cell optical imaging and spectroscopy. *Chem. Rev*. 113:2469–527
54. Gu Y, Ha JW, Augspurger AE, Chen K, Zhu S, Fang N. 2013. Single Particle Orientation and Rotational Tracking (SPORT) in biophysical studies. *Nanoscale* 5:10753–64
55. Waga S, Stillman B. 1998. The DNA replication fork in eukaryotic cells. *Annu. Rev. Biochem.* 67:721–51
56. Fass D, Bogden CE, Berger JM. 1999. Quaternary changes in topoisomerase II may direct orthogonal movement of two DNA strands. *Nat. Struct. Biol.* 6:322–6
57. Yasuda R, Noji H, Yoshida M, Kinosita K, Itoh H. 2001. Resolution of distinct rotational substeps by submillisecond kinetic analysis of F_1-ATPase. *Nature* 410:898–904
58. Cingolani G, Duncan TM. 2011. Structure of the ATP synthase catalytic complex (F_1) from *Escherichia coli* in an autoinhibited conformation. *Nat. Struct. Mol. Biol.* 18:701–7
59. Forkey JN, Quinlan ME, Alexander Shaw M, Corrie JET, Goldman YE. 2003. Three-dimensional structural dynamics of myosin V by single-molecule fluorescence polarization. *Nature* 422:399–404
60. Kural C, Kim H, Syed S, Goshima G, Gelfand VI, Selvin PR. 2005. Kinesin and dynein move a peroxisome in vivo: a tug-of-war or coordinated movement? *Science* 308:1469–72
61. Guo P, Noji H, Yengo CM, Zhao Z, Grainge I. 2016. Biological nanomotors with a revolution, linear, or rotation motion mechanism. *Microbiol. Mol. Biol. Rev.* 80:161–86
62. Enoki S, Iino R, Niitani Y, Minagawa Y, Tomishige M, Noji H. 2015. High-speed angle-resolved imaging of a single gold nanorod with microsecond temporal resolution and one-degree angle precision. *Anal. Chem.* 87:2079–86
63. Shroder DY, Lippert LG, Goldman YE. 2016. Single molecule optical measurements of orientation and rotations of biological macromolecules. *Methods Appl. Fluoresc.* 4:042004
64. Toprak E, Enderlein J, Syed S, McKinney SA, Petschek RG, et al. 2006. Defocused orientation and position imaging (DOPI) of myosin V. *PNAS* 103:6495–99
65. Zhang O, Lu J, Ding T, Lew MD. 2019. Erratum: "Imaging the three-dimensional orientation and rotational mobility of fluorescent emitters using the Tri-spot point spread function" [Appl. Phys. Lett. 113, 031103 2018]. *Appl. Phys. Lett.* 115:069901
66. Zhang O, Lew MD. 2019. Fundamental limits on measuring the rotational constraint of single molecules using fluorescence microscopy. *Phys. Rev. Lett.* 122:198301
67. Ha T, Enderle T, Chemla DS, Selvin PR, Weiss S. 1996. Single molecule dynamics studied by polarization modulation. *Phys. Rev. Lett.* 77:3979–82
68. Fourkas JT. 2001. Rapid determination of the three-dimensional orientation of single molecules. *Opt. Lett.* 26:211–13

69. Böhmer M, Enderlein J. 2003. Orientation imaging of single molecules by wide-field epifluorescence microscopy. *J. Opt. Soc. Am. B* 20:554–59
70. Lieb MA, Zavislan JM, Novotny L. 2004. Single-molecule orientations determined by direct emission pattern imaging. *J. Opt. Soc. Am. B* 21:1210–15
71. Sikorski Z, Davis LM. 2008. Engineering the collected field for single-molecule orientation determination. *Opt. Express* 16:3660–73
72. Backer AS, Moerner WE. 2015. Determining the rotational mobility of a single molecule from a single image: a numerical study. *Opt. Express* 23:4255–76
73. Backer AS, Lee MY, Moerner WE. 2016. Enhanced DNA imaging using super-resolution microscopy and simultaneous single-molecule orientation measurements. *Optica* 3:659–66
74. Li Q, Chen X-J, Xu Y, Lan S, Liu H-Y, et al. 2010. Photoluminescence properties of the CdSe quantum dots accompanied with rotation of the defocused wide-field fluorescence images. *J. Phys. Chem. C* 114:13427–32
75. Kukura P, Ewers H, Müller C, Renn A, Helenius A, Sandoghdar V. 2009. High-speed nanoscopic tracking of the position and orientation of a single virus. *Nat. Methods* 6:923–27
76. Ohmachi M, Komori Y, Iwane AH, Fujii F, Jin T, Yanagida T. 2012. Fluorescence microscopy for simultaneous observation of 3D orientation and movement and its application to quantum rod-tagged myosin V. *PNAS* 109:5294–98
77. Forkey JN, Quinlan ME, Goldman YE. 2001. Protein structural dynamics by single-molecule fluorescence polarization. In *Biology at the Single-Molecule Level*, ed. SH Leuba, J Zlatanova, pp. 1–35. Amsterdam: Pergamon
78. Peterman EJG, Sosa H, Moerner WE. 2004. Single-molecule fluorescence spectroscopy and microscopy of biomolecular motors. *Annu. Rev. Phys. Chem.* 55:79–96
79. Rosenberg SA, Quinlan ME, Forkey JN, Goldman YE. 2005. Rotational motions of macro-molecules by single-molecule fluorescence microscopy. *Acc. Chem. Res.* 38:583–93
80. Jain PK, Huang X, El-Sayed IH, El-Sayed MA. 2008. Noble metals on the nanoscale: optical and photothermal properties and some applications in imaging, sensing, biology, and medicine. *Acc. Chem. Res.* 41:1578–86
81. Olson J, Dominguez-Medina S, Hoggard A, Wang L-Y, Chang W-S, Link S. 2015. Optical characterization of single plasmonic nanoparticles. *Chem. Soc. Rev.* 44:40–57
82. Xiao L, Yeung ES. 2014. Optical imaging of individual plasmonic nanoparticles in biological samples. *Annu. Rev. Anal. Chem.* 7:89–111
83. Peng Y, Xiong B, Peng L, Li H, He Y, Yeung ES. 2015. Recent advances in optical imaging with anisotropic plasmonic nanoparticles. *Anal. Chem.* 87:200–15
84. Ha JW. 2016. Recent advances in single particle rotational tracking of plasmonic anisotropic gold nanoparticles under far-field optical microscopy. *Appl. Spectrosc. Rev.* 51:552–69
85. Ma Y, Wang X, Liu H, Wei L, Xiao L. 2019. Recent advances in optical microscopic methods for single-particle tracking in biological samples. *Anal. Bioanal. Chem.* 411:4445–63
86. Wu Y, Ali MRK, Chen K, Fang N, El-Sayed MA. 2019. Gold nanoparticles in biological optical imaging. *NanoToday* 24:120–40
87. Wang G, Stender AS, Sun W, Fang N. 2010. Optical imaging of non-fluorescent nanoparticle probes in live cells. *Analyst* 135:215–21
88. Rong G, Wang H, Reinhard BM. 2010. Insights from a nanoparticle minuet: two-dimensional membrane profiling through silver plasmon ruler tracking. *Nano Lett.* 10:230–38
89. Ha JW, Chen K, Fang N. 2013. Differential interference contrast microscopy imaging of micrometer-long plasmonic nanowires. *Chem. Commun.* 49:11038–40
90. Culver KSB, Liu T, Hryn AJ, Fang N, Odom TW. 2018. *In situ* identification of nanoparticle structural information using optical microscopy. *J. Phys. Chem. Lett.* 9:2886–92
91. Jeon HB, Tsalu PV, Ha JW. 2019. Shape effect on the refractive index sensitivity at localized surface plasmon resonance inflection points of single gold nanocubes with vertices. *Sci. Rep.* 9:13635
92. Lee SY, Tsalu PV, Kim GW, Seo MJ, Hong JW, Ha JW. 2019. Tuning chemical interface damping: interfacial electronic effects of adsorbate molecules and sharp tips of single gold bipyramids. *Nano Lett.* 19:2568–74

93. Kaplan L, Ierokomos A, Chowdary P, Bryant Z, Cui B. 2018. Rotation of endosomes demonstrates coordination of molecular motors during axonal transport. *Sci. Adv.* 4:e1602170
94. Kim GW, Ha JW. 2018. Direct visualization of wavelength-dependent single dipoles generated on single gold nanourchins with sharp branches. *Nanoscale Res. Lett.* 13:256
95. Lee J, Ha JW. 2018. Elucidating the contribution of dipole resonance mode to polarization-dependent optical properties in single triangular gold nanoplates. *Chem. Phys. Lett.* 713:121–24
96. Lee SY, Han Y, Hong JW, Ha JW. 2017. Single gold bipyramids with sharp tips as sensitive single particle orientation sensors in biological studies. *Nanoscale* 9:12060–67
97. Lee J, Ha JW. 2019. Single-particle correlation study: polarization-dependent differential interference contrast imaging of two-dimensional gold nanoplates. *Anal. Sci.* 35:1237–41
98. Lee J, Ha JW. 2017. Defocused dark-field orientation imaging of single gold microrods on synthetic membranes. *Phys. Chem. Chem. Phys.* 19:24453–57
99. Stender AS, Wei X, Augspurger AE, Fang N. 2013. Plasmonic behavior of single gold dumbbells and simple dumbbell geometries. *J. Phys. Chem. C* 117:16195–202
100. Sönnichsen C, Alivisatos AP. 2005. Gold nanorods as novel nonbleaching plasmon-based orientation sensors for polarized single-particle microscopy. *Nano Lett.* 5:301–4
101. Chang W-S, Ha JW, Slaughter LS, Link S. 2010. Plasmonic nanorod absorbers as orientation sensors. *PNAS* 107:2781–86
102. Stender AS, Wang G, Sun W, Fang N. 2010. Influence of gold nanorod geometry on optical response. *ACS Nano* 4:7667–75
103. Chen H, Shao L, Li Q, Wang J. 2013. Gold nanorods and their plasmonic properties. *Chem. Soc. Rev.* 42:2679–724
104. Ha JW, Sun W, Wang G, Fang N. 2011. Differential interference contrast polarization anisotropy for tracking rotational dynamics of gold nanorods. *Chem. Commun.* 47:7743–45
105. Gu Y, Di X, Sun W, Wang G, Fang N. 2012. Three-dimensional super-localization and tracking of single gold nanoparticles in cells. *Anal. Chem.* 84:4111–17
106. Gu Y, Sun W, Wang G, Jeftinija K, Jeftinija S, Fang N. 2012. Rotational dynamics of cargos at pauses during axonal transport. *Nat. Commun.* 3:1030
107. Ha JW, Sun W, Stender AS, Fang N. 2012. Dual-wavelength detection of rotational diffusion of single anisotropic nanocarriers on live cell membranes. *J. Phys. Chem. C* 116:2766–71
108. Sun W, Gu Y, Wang G, Fang N. 2012. Dual-modality single particle orientation and rotational tracking of intracellular transport of nanocargos. *Anal. Chem.* 84:1134–38
109. Gu Y, Sun W, Wang G, Zimmermann MT, Jernigan RL, Fang N. 2013. Revealing rotational modes of functionalized gold nanorods on live cell membranes. *Small* 9:785
110. Gu Y, Wang G, Fang N. 2013. Simultaneous single-particle superlocalization and rotational tracking. *ACS Nano* 7:1658–65
111. Wei L, Xu J, Ye Z, Zhu X, Zhong M, et al. 2016. Orientational imaging of a single gold nanorod at the liquid/solid interface with polarized evanescent field illumination. *Anal. Chem.* 88:1995–99
112. Xu D, He Y, Yeung ES. 2014. Direct observation of the orientation dynamics of single protein-coated nanoparticles at liquid/solid interfaces. *Angew. Chem. Int. Ed.* 53:6951–55
113. Xiao L, Qiao Y, He Y, Yeung ES. 2011. Imaging translational and rotational diffusion of single anisotropic nanoparticles with planar illumination microscopy. *J. Am. Chem. Soc.* 133:10638–45
114. Xiao L, Qiao Y, He Y, Yeung ES. 2010. Three dimensional orientational imaging of nanoparticles with darkfield microscopy. *Anal. Chem.* 82:5268–74
115. Chowdary PD, Kaplan L, Che DL, Cui B. 2018. Dynamic clustering of dyneins on axonal endosomes: evidence from high-speed darkfield imaging. *Biophys. J.* 115:230–41
116. Xu D, He Y, Yeung ES. 2014. Direct imaging of transmembrane dynamics of single nanoparticles with darkfield microscopy: improved orientation tracking at cell sidewall. *Anal. Chem.* 86:3397–404
117. Xiao L, Wei L, Liu C, He Y, Yeung ES. 2012. Unsynchronized translational and rotational diffusion of nanocargo on a living cell membrane. *Angew. Chem. Int. Ed.* 51:4181–84
118. Ha JW, Marchuk K, Fang N. 2012. Focused orientation and position imaging (FOPI) of single anisotropic plasmonic nanoparticles by total internal reflection scattering microscopy. *Nano Lett.* 12:4282–88

119. Marchuk K, Ha JW, Fang N. 2013. Three-dimensional high-resolution rotational tracking with super-localization reveals conformations of surface-bound anisotropic nanoparticles. *Nano Lett.* 13:1245–50
120. Marchuk K, Fang N. 2013. Three-dimensional orientation determination of stationary anisotropic nanoparticles with sub-degree precision under total internal reflection scattering microscopy. *Nano Lett.* 13:5414–19
121. Tcherniak A, Dominguez-Medina S, Chang W-S, Swanglap P, Slaughter LS, et al. 2011. One-photon plasmon luminescence and its application to correlation spectroscopy as a probe for rotational and translational dynamics of gold nanorods. *J. Phys. Chem. C* 115:15938–49
122. Zhang B, Lan T, Huang X, Dong C, Ren J. 2013. Sensitive single particle method for characterizing rapid rotational and translational diffusion and aspect ratio of anisotropic nanoparticles and its application in immunoassays. *Anal. Chem.* 85:9433–38
123. Sun W, Wang G, Fang N, Yeung ES. 2009. Wavelength-dependent differential interference contrast microscopy: selectively imaging nanoparticle probes in live cells. *Anal. Chem.* 81:9203–8
124. Luo Y, Sun W, Gu Y, Wang G, Fang N. 2010. Wavelength-dependent differential interference contrast microscopy: multiplexing detection using nonfluorescent nanoparticles. *Anal. Chem.* 82:6675–79
125. Stender AS, Augspurger AE, Wang G, Fang N. 2012. Influence of polarization setting on gold nanorod signal at nonplasmonic wavelengths under differential interference contrast microscopy. *Anal. Chem.* 84:5210–15
126. Chen K, Lin C-C, Vela J, Fang N. 2015. Multishell Au/Ag/SiO_2 nanorods with tunable optical properties as single particle orientation and rotational tracking probes. *Anal. Chem.* 87:4096–99
127. Pan Q, Zhao H, Lin X, He Y. 2019. Spatiotemporal heterogeneity of reactions in solution observed with high-speed single-nanorod rotational sensing. *Angew. Chem. Int. Ed.* 58:8389–93
128. Kim GW, Lee SY, Ha JW. 2017. Three-dimensional defocused orientation sensing of single bimetallic core–shell gold nanorods as multifunctional optical probes. *Analyst* 142:899–903
129. Kim GW, Ha JW. 2017. Platinum-coated core-shell gold nanorods as multifunctional orientation sensors in differential interference contrast microscopy. *Anal. Sci.* 33:1021–25
130. Xiong B, Zhou R, Hao J, Jia Y, He Y, Yeung ES. 2013. Highly sensitive sulphide mapping in live cells by kinetic spectral analysis of single Au-Ag core-shell nanoparticles. *Nat. Commun.* 4:1708
131. Zhao F, Chen K, Dong B, Yang K, Gu Y, Fang N. 2017. Localization accuracy of gold nanoparticles in single particle orientation and rotational tracking. *Opt. Express* 25:9860–71
132. Cheng X, Chen K, Dong B, Filbrun SL, Wang G, Fang N. 2021. Resolving cargo-motor-track interactions with bifocal parallax single-particle tracking. *Biophys. J.* 120:1378–86
133. Cheng X, Chen K, Dong B, Yang M, Filbrun S, et al. 2021. Dynamin-dependent vesicle twist at the final stage of clathrin-mediated endocytosis. *Nat. Cell Biol.* 23:859–69
134. Lattuada M, Hatton TA. 2011. Synthesis, properties and applications of Janus nanoparticles. *Nano Today* 6:286–308
135. Walther A, Müller AHE. 2013. Janus particles: synthesis, self-assembly, physical properties, and applications. *Chem. Rev.* 113:5194–261
136. Anker JN, Behrend C, Kopelman R. 2003. Aspherical magnetically modulated optical nanoprobes (MagMOONs). *J. Appl. Phys.* 93:6698–700
137. Anker JN, Kopelman R. 2003. Magnetically modulated optical nanoprobes. *Appl. Phys. Lett.* 82:1102–4
138. Anthony SM, Hong L, Kim M, Granick S. 2006. Single-particle colloid tracking in four dimensions. *Langmuir* 22:9812–15
139. Anthony SM, Yu Y. 2015. Tracking single particle rotation: probing dynamics in four dimensions. *Anal. Methods* 7:7020–28
140. Nguyen KT, Anker JN. 2014. Detecting de-gelation through tissue using magnetically modulated optical nanoprobes (MagMOONs). *Sens. Actuators B Chem.* 205:313–21
141. Sanchez L, Patton P, Anthony SM, Yi Y, Yu Y. 2015. Tracking single-particle rotation during macrophage uptake. *Soft Matter* 11:5346–52
142. Gao Y, Yu Y, Sanchez L, Yu Y. 2017. Seeing the unseen: imaging rotation in cells with designer anisotropic particles. *Micron* 101:123–31
143. Gao Y, Anthony SM, Yi Y, Li W, Yu Y, Yu Y. 2018. Single-Janus rod tracking reveals the "rock-and-roll" of endosomes in living cells. *Langmuir* 34:1151–58

144. Gao Y, Anthony SM, Yu Y, Yi Y, Yu Y. 2018. Cargos rotate at microtubule intersections during intracellular trafficking. *Biophys. J.* 114:2900–9
145. Lee K, Zhang L, Yi Y, Wang X, Yu Y. 2018. Rupture of lipid membranes induced by amphiphilic Janus nanoparticles. *ACS Nano* 12:3646–57
146. Yu Y, Gao Y, Yu Y. 2018. "Waltz" of cell membrane-coated nanoparticles on lipid bilayers: tracking single particle rotation in ligand–receptor binding. *ACS Nano* 12:11871–80
147. Lee K, Yu Y. 2019. Lipid bilayer disruption induced by amphiphilic Janus nanoparticles: the non-monotonic effect of charged lipids. *Soft Matter* 15:2373–80
148. Li W, Wojcik M, Xu K. 2019. Optical microscopy unveils rapid, reversible electrochemical oxidation and reduction of graphene. *Nano Lett.* 19:983–89
149. Chen X, Shen Z, He Y, Guan T, He Q, et al. 2019. Dual-wavelength digital holographic phase and fluorescence microscopy combining with Raman spectroscopy for micro-quartz pieces-based dual-channel encoded suspension array. *Opt. Express* 27:1894–910
150. Choi Y-W, Mistry H, Cuenya BR. 2017. New insights into working nanostructured electrocatalysts through operando spectroscopy and microscopy. *Curr. Opin. Electrochem.* 1:95–103
151. Gong Z, Pan Y-L, Videen G, Wang C. 2018. Optical trapping-Raman spectroscopy (OT-RS) with embedded microscopy imaging for concurrent characterization and monitoring of physical and chemical properties of single particles. *Anal. Chim. Acta* 1020:86–94
152. Yang Y-C, Chang W-T, Huang S-K, Liau I. 2014. Characterization of the pharmaceutical effect of drugs on atherosclerotic lesions *in vivo* using integrated fluorescence imaging and Raman spectral measurements. *Anal. Chem.* 86:3863–68
153. Kong K, Rowlands CJ, Varma S, Perkins W, Leach IH, et al. 2013. Diagnosis of tumors during tissue-conserving surgery with integrated autofluorescence and Raman scattering microscopy. *PNAS* 110:15189–94
154. Jhan J-W, Chang W-T, Chen H-C, Lee Y-T, Wu M-F, et al. 2008. Integrated multiple multi-photon imaging and Raman spectroscopy for characterizing structure-constituent correlation of tissues. *Opt. Express* 16:16431–41
155. Nallala J, Piot O, Diebold M-D, Gobinet C, Bouché O, et al. 2014. Infrared and Raman imaging for characterizing complex biological materials: a comparative morpho-spectroscopic study of colon tissue. *Appl. Spectrosc.* 68:57–68
156. Depciuch J, Kaznowska E, Zawlik I, Wojnarowska R, Cholewa M, et al. 2016. Application of Raman spectroscopy and infrared spectroscopy in the identification of breast cancer. *Appl. Spectrosc.* 70:251–63
157. Perez-Guaita D, Kochan K, Martin M, Andrew DW, Heraud P, et al. 2017. Multimodal vibrational imaging of cells. *Vib. Spectrosc.* 91:46–58
158. Kochan K, Peng H, Wood BR, Haritos VS. 2018. Single cell assessment of yeast metabolic engineering for enhanced lipid production using Raman and AFM-IR imaging. *Biotechnol. Biofuels* 11:106
159. Dazzi A, Prater CB, Hu Q, Chase DB, Rabolt JF, Marcott C. 2012. AFM–IR: combining atomic force microscopy and infrared spectroscopy for nanoscale chemical characterization. *Appl. Spectrosc.* 66:1365–84
160. Zhang D, Li C, Zhang C, Slipchenko MN, Eakins G, Cheng J-X. 2016. Depth-resolved mid-infrared photothermal imaging of living cells and organisms with submicrometer spatial resolution. *Sci. Adv.* 2:e1600521
161. Li C, Zhang D, Slipchenko MN, Cheng J-X. 2017. Mid-infrared photothermal imaging of active pharmaceutical ingredients at submicrometer spatial resolution. *Anal. Chem.* 89:4863–67
162. Bai Y, Zhang D, Li C, Liu C, Cheng J-X. 2017. Bond-selective imaging of cells by mid-infrared photothermal microscopy in high wavenumber region. *J. Phys. Chem. B* 121:10249–55
163. Li Z, Aleshire K, Kuno M, Hartland GV. 2017. Super-resolution far-field infrared imaging by photothermal heterodyne imaging. *J. Phys. Chem. B* 121:8838–46
164. Li X, Zhang D, Bai Y, Wang W, Liang J, Cheng J-X. 2019. Fingerprinting a living cell by Raman integrated mid-infrared photothermal microscopy. *Anal. Chem.* 91:10750–56
165. Bossi M, Fölling J, Belov VN, Boyarskiy VP, Medda R, et al. 2008. Multicolor far-field fluorescence nanoscopy through isolated detection of distinct molecular species. *Nano Lett.* 8:2463–68

166. Testa I, Wurm CA, Medda R, Rothermel E, von Middendorf C, et al. 2010. Multicolor fluorescence nanoscopy in fixed and living cells by exciting conventional fluorophores with a single wavelength. *Biophys. J.* 99:2686–94
167. Gunewardene MS, Subach FV, Gould TJ, Penoncello GP, Gudheti MV, et al. 2011. Superresolution imaging of multiple fluorescent proteins with highly overlapping emission spectra in living cells. *Biophys. J.* 101:1522–28
168. Zhang Z, Kenny SJ, Hauser M, Li W, Xu K. 2015. Ultrahigh-throughput single-molecule spectroscopy and spectrally resolved super-resolution microscopy. *Nat. Methods* 12:935–38
169. Mlodzianoski MJ, Curthoys NM, Gunewardene MS, Carter S, Hess ST. 2016. Super-resolution imaging of molecular emission spectra and single molecule spectral fluctuations. *PLOS ONE* 11:e0147506-e
170. Comtet J, Glushkov E, Navikas V, Feng J, Babenko V, et al. 2019. Wide-field spectral super-resolution mapping of optically active defects in hexagonal boron nitride. *Nano Lett.* 19:2516–23
171. Moon S, Yan R, Kenny SJ, Shyu Y, Xiang L, et al. 2017. Spectrally resolved, functional super-resolution microscopy reveals nanoscale compositional heterogeneity in live-cell membranes. *J. Am. Chem. Soc.* 139:10944–47
172. Dong B, Almassalha L, Urban BE, Nguyen T-Q, Khuon S, et al. 2016. Super-resolution spectroscopic microscopy via photon localization. *Nat. Commun.* 7:12290
173. Bongiovanni MN, Godet J, Horrocks MH, Tosatto L, Carr AR, et al. 2016. Multi-dimensional super-resolution imaging enables surface hydrophobicity mapping. *Nat. Commun.* 7:13544
174. Kim D, Zhang Z, Xu K. 2017. Spectrally resolved super-resolution microscopy unveils multipath reaction pathways of single spiropyran molecules. *J. Am. Chem. Soc.* 139:9447–50
175. Zhao F, Filbrun SL, Huang T, Dong B, Fang N. 2021. Multiscale evolution of bulk heterojunction solar cell active layers under thermal stress. *Anal. Chem.* 93:1232–36
176. Berera R, van Grondelle R, Kennis JTM. 2009. Ultrafast transient absorption spectroscopy: principles and application to photosynthetic systems. *Photosynth. Res.* 101:105–18
177. Jones AC, Kearns NM, Ho J-J, Flach JT, Zanni MT. 2020. Impact of non-equilibrium molecular packings on singlet fission in microcrystals observed using 2D white-light microscopy. *Nat. Chem.* 12:40–47
178. Jones AC, Kearns NM, Bohlmann Kunz M, Flach JT, Zanni MT. 2019. Multidimensional spectroscopy on the microscale: development of a multimodal imaging system incorporating 2D white-light spectroscopy, broadband transient absorption, and atomic force microscopy. *J. Phys. Chem. A* 123:10824–36
179. Wang X, Huang S-C, Huang T-X, Su H-S, Zhong J-H, et al. 2017. Tip-enhanced Raman spectroscopy for surfaces and interfaces. *Chem. Soc. Rev.* 46:4020–41
180. Huang T-X, Cong X, Wu S-S, Lin K-Q, Yao X, et al. 2019. Probing the edge-related properties of atomically thin MoS_2 at nanoscale. *Nat. Commun.* 10:5544
181. Zeng Z-C, Huang S-C, Wu D-Y, Meng L-Y, Li M-H, et al. 2015. Electrochemical tip-enhanced Raman spectroscopy. *J. Am. Chem. Soc.* 137:11928–31
182. Park K-D, Khatib O, Kravtsov V, Clark G, Xu X, Raschke MB. 2016. Hybrid tip-enhanced nanospectroscopy and nanoimaging of monolayer WSe_2 with local strain control. *Nano Lett.* 16:2621–27
183. Tang C, Jia S, Chen W, Lou J, Voronine DV. 2017. Nano-optical imaging of monolayer MoSe2 using tip-enhanced photoluminescence. arXiv:1704.02396v2 [physics.optics]
184. Huth F, Govyadinov A, Amarie S, Nuansing W, Keilmann F, Hillenbrand R. 2012. Nano-FTIR absorption spectroscopy of molecular fingerprints at 20 nm spatial resolution. *Nano Lett.* 12:3973–78
185. Fei Z, Rodin AS, Andreev GO, Bao W, McLeod AS, et al. 2012. Gate-tuning of graphene plasmons revealed by infrared nano-imaging. *Nature* 487:82–85
186. van Schrojenstein Lantman EM, Deckert-Gaudig T, Mank AJG, Deckert V, Weckhuysen BM. 2012. Catalytic processes monitored at the nanoscale with tip-enhanced Raman spectroscopy. *Nat. Nanotechnol.* 7:583–86
187. Zhang R, Zhang Y, Dong ZC, Jiang S, Zhang C, et al. 2013. Chemical mapping of a single molecule by plasmon-enhanced Raman scattering. *Nature* 498:82–86
188. Hoffman DP, Shtengel G, Xu CS, Campbell KR, Freeman M, et al. 2020. Correlative three-dimensional super-resolution and block-face electron microscopy of whole vitreously frozen cells. *Science* 367:eaaz5357

189. Matusovsky OS, Mansson A, Persson M, Cheng Y-S, Rassier DE. 2019. High-speed AFM reveals subsecond dynamics of cardiac thin filaments upon Ca^{2+} activation and heavy meromyosin binding. *PNAS* 116:16384–93
190. Petti MK, Lomont JP, Maj M, Zanni MT. 2018. Two-dimensional spectroscopy is being used to address core scientific questions in biology and materials science. *J. Phys. Chem. B* 122:1771–80
191. Lomont JP, Ostrander JS, Ho J-J, Petti MK, Zanni MT. 2017. Not all β-sheets are the same: amyloid infrared spectra, transition dipole strengths, and couplings investigated by 2D IR spectroscopy. *J. Phys. Chem. B* 121:8935–45
192. Dunkelberger EB, Grechko M, Zanni MT. 2015. Transition dipoles from 1D and 2D infrared spectroscopy help reveal the secondary structures of proteins: application to amyloids. *J. Phys. Chem. B* 119:14065–75
193. Kearns NM, Mehlenbacher RD, Jones AC, Zanni MT. Broadband 2D electronic spectrometer using white light and pulse shaping: noise and signal evaluation at 1 and 100 kHz. *Opt. Express* 25:7869–83
194. Hamm P. 2014. 2D-Raman-THz spectroscopy: a sensitive test of polarizable water models. *J. Chem. Phys.* 141:184201
195. Shalit A, Ahmed S, Savolainen J, Hamm P. 2017. Terahertz echoes reveal the inhomogeneity of aqueous salt solutions. *Nat. Chem.* 9:273–78
196. Courtney TL, Fox ZW, Slenkamp KM, Lynch MS, Khalil M. 2015. Two-dimensional Fourier transform infrared-visible and infrared-Raman spectroscopies. In *Ultrafast Phenomena XIX*, ed. K Yamanouchi, S Cundiff, R de Vivie-Riedle, M Kuwata-Gonokami, L DiMauro, pp. 503–5. Springer Proc. Phys., Vol. 162. Cham, Switz.: Springer Int.
197. Newby JM, Schaefer AM, Lee PT, Forest MG, Lai SK. 2018. Convolutional neural networks automate detection for tracking of submicron-scale particles in 2D and 3D. *PNAS* 115:9026–31
198. Zhong Y, Li C, Zhou H, Wang G. 2018. Developing noise-resistant three-dimensional single particle tracking using deep neural networks. *Anal. Chem.* 90:10748–57
199. Christiansen EM, Yang SJ, Ando DM, Javaherian A, Skibinski G, et al. 2018. *In silico* labeling: predicting fluorescent labels in unlabeled images. *Cell* 173:792–803.e19